Constraints on the extremely-high energy cosmic neutrino flux with the IceCube 2008-2009 data

R. Abbasi,[28] Y. Abdou,[22] T. Abu-Zayyad,[33] J. Adams,[16] J. A. Aguilar,[28] M. Ahlers,[32] K. Andeen,[28] J. Auffenberg,[38] X. Bai,[31] M. Baker,[28] S. W. Barwick,[24] R. Bay,[7] J. L. Bazo Alba,[39] K. Beattie,[8] J. J. Beatty,[18,19] S. Bechet,[13] J. K. Becker,[10] K.-H. Becker,[38] M. L. Benabderrahmane,[39] S. BenZvi,[28] J. Berdermann,[39] P. Berghaus,[28] D. Berley,[17] E. Bernardini,[39] D. Bertrand,[13] D. Z. Besson,[26] D. Bindig,[38] M. Bissok,[1] E. Blaufuss,[17] J. Blumenthal,[1] D. J. Boersma,[1] C. Bohm,[34] D. Bose,[14] S. Böser,[11] O. Botner,[37] J. Braun,[28] A. M. Brown,[16] S. Buitink,[8] M. Carson,[22] D. Chirkin,[28] B. Christy,[17] J. Clem,[31] F. Clevermann,[20] S. Cohen,[25] C. Colnard,[23] D. F. Cowen,[36,35] M. V. D'Agostino,[7] M. Danninger,[34] J. Daughhetee,[5] J. C. Davis,[18] C. De Clercq,[14] L. Demirörs,[25] T. Denger,[11] O. Depaepe,[14] F. Descamps,[22] P. Desiati,[28] G. de Vries-Uiterweerd,[22] T. DeYoung,[36] J. C. Díaz-Vélez,[28] M. Dierckxsens,[13] J. Dreyer,[10] J. P. Dumm,[28] R. Ehrlich,[17] J. Eisch,[28] R. W. Ellsworth,[17] O. Engdegård,[37] S. Euler,[1] P. A. Evenson,[31] O. Fadiran,[4] A. R. Fazely,[6] A. Fedynitch,[10] T. Feusels,[22] K. Filimonov,[7] C. Finley,[34] T. Fischer-Wasels,[38] M. M. Foerster,[36] B. D. Fox,[36] A. Franckowiak,[11] R. Franke,[39] T. K. Gaisser,[31] J. Gallagher,[27] M. Geisler,[1] L. Gerhardt,[8,7] L. Gladstone,[28] T. Glüsenkamp,[1] A. Goldschmidt,[8] J. A. Goodman,[17] D. Gora,[39] D. Grant,[21] T. Griesel,[29] A. Groß,[16,23] S. Grullon,[28] M. Gurtner,[38] C. Ha,[36] A. Hallgren,[37] F. Halzen,[28] K. Han,[39] K. Hanson,[13,28] D. Heinen,[1] K. Helbing,[38] P. Herquet,[30] S. Hickford,[16] G. C. Hill,[28] K. D. Hoffman,[17] A. Homeier,[11] K. Hoshina,[28] D. Hubert,[14] W. Huelsnitz,[17] J.-P. Hülß,[1] P. O. Hulth,[34] K. Hultqvist,[34] S. Hussain,[31] A. Ishihara,[15,*] J. Jacobsen,[28] G. S. Japaridze,[4] H. Johansson,[34] J. M. Joseph,[8] K.-H. Kampert,[38] A. Kappes,[9] T. Karg,[38] A. Karle,[28] J. L. Kelley,[28] P. Kenny,[26] J. Kiryluk,[8,7] F. Kislat,[39] S. R. Klein,[8,7] J.-H. Köhne,[20] G. Kohnen,[30] H. Kolanoski,[9] L. Köpke,[29] S. Kopper,[38] D. J. Koskinen,[36] M. Kowalski,[11] T. Kowarik,[29] M. Krasberg,[28] T. Krings,[1] G. Kroll,[29] T. Kuwabara,[31] M. Labare,[14] S. Lafebre,[36] K. Laihem,[1] H. Landsman,[28] M. J. Larson,[36] R. Lauer,[39] J. Lünemann,[29] J. Madsen,[33] P. Majumdar,[39] A. Marotta,[13] R. Maruyama,[28] K. Mase,[15] H. S. Matis,[8] K. Meagher,[17] M. Merck,[28] P. Mészáros,[35,36] T. Meures,[1] E. Middell,[39] N. Milke,[20] J. Miller,[37] T. Montaruli,[28,†] R. Morse,[28] S. M. Movit,[35] R. Nahnhauer,[39] J. W. Nam,[24] U. Naumann,[38] P. Nießen,[31] D. R. Nygren,[8] S. Odrowski,[23] A. Olivas,[17] M. Olivo,[10] A. O'Murchadha,[28] M. Ono,[15] S. Panknin,[11] L. Paul,[1] C. Pérez de los Heros,[37] J. Petrovic,[13] A. Piegsa,[29] D. Pieloth,[20] R. Porrata,[7] J. Posselt,[38] P. B. Price,[7] G. T. Przybylski,[8] K. Rawlins,[3] P. Redl,[17] E. Resconi,[23] W. Rhode,[20] M. Ribordy,[25] A. Rizzo,[14] J. P. Rodrigues,[28] P. Roth,[17] F. Rothmaier,[29] C. Rott,[18] T. Ruhe,[20] D. Rutledge,[36] B. Ruzybayev,[31] D. Ryckbosch,[22] H.-G. Sander,[29] M. Santander,[28] S. Sarkar,[32] K. Schatto,[29] T. Schmidt,[17] A. Schönwald,[39] A. Schukraft,[1] A. Schultes,[38] O. Schulz,[23] M. Schunck,[1] D. Seckel,[31] B. Semburg,[38] S. H. Seo,[34] Y. Sestayo,[23] S. Seunarine,[12] A. Silvestri,[24] A. Slipak,[36] G. M. Spiczak,[33] C. Spiering,[39] M. Stamatikos,[18,‡] T. Stanev,[31] G. Stephens,[36] T. Stezelberger,[8] R. G. Stokstad,[8] A. Stössl,[39] S. Stoyanov,[31] E. A. Strahler,[14] T. Straszheim,[17] M. Stür,[11] G. W. Sullivan,[17] Q. Swillens,[13] H. Taavola,[37] I. Taboada,[5] A. Tamburro,[33] A. Tepe,[5] S. Ter-Antonyan,[6] S. Tilav,[31] P. A. Toale,[2] S. Toscano,[28] D. Tosi,[39] D. Turčan,[17] N. van Eijndhoven,[14] J. Vandenbroucke,[7] A. Van Overloop,[22] J. van Santen,[28] M. Vehring,[1] M. Voge,[11] C. Walck,[34] T. Waldenmaier,[9] M. Wallraff,[1] M. Walter,[39] Ch. Weaver,[28] C. Wendt,[28] S. Westerhoff,[28] N. Whitehorn,[28] K. Wiebe,[29] C. H. Wiebusch,[1] D. R. Williams,[2] R. Wischnewski,[39] H. Wissing,[17] M. Wolf,[23] T. R. Wood,[21] K. Woschnagg,[7] C. Xu,[31] X. W. Xu,[6] G. Yodh,[24] S. Yoshida,[15] and P. Zarzhitsky[2]

(IceCube Collaboration)

[1]*III. Physikalisches Institut, RWTH Aachen University, D-52056 Aachen, Germany*
[2]*Department of Physics and Astronomy, University of Alabama, Tuscaloosa, Alabama 35487, USA*
[3]*Department of Physics and Astronomy, University of Alaska Anchorage, 3211 Providence Dr., Anchorage, Alaska 99508, USA*
[4]*CTSPS, USAClark-Atlanta University, Atlanta, Georgia 30314, USA*
[5]*School of Physics and Center for Relativistic Astrophysics, Georgia Institute of Technology, Atlanta, Georgia 30332, USA*
[6]*Department of Physics, Southern University, Baton Rouge, Louisiana 70813, USA*
[7]*Department of Physics, University of California, Berkeley, California 94720, USA*
[8]*Lawrence Berkeley National Laboratory, Berkeley, California 94720, USA*
[9]*Institut für Physik, Humboldt-Universität zu Berlin, D-12489 Berlin, Germany*
[10]*Fakultät für Physik & Astronomie, Ruhr-Universität Bochum, D-44780 Bochum, Germany*
[11]*Physikalisches Institut, Universität Bonn, Nussallee 12, D-53115 Bonn, Germany*
[12]*Department of Physics, University of the West Indies, Cave Hill Campus, Bridgetown BB11000, Barbados*
[13]*Université Libre de Bruxelles, Science Faculty CP230, B-1050 Brussels, Belgium*
[14]*Vrije Universiteit Brussel, Dienst ELEM, B-1050 Brussels, Belgium*
[15]*Department of Physics, Chiba University, Chiba 263-8522, Japan*
[16]*Department of Physics and Astronomy, University of Canterbury, Private Bag 4800, Christchurch, New Zealand*

^{17}*Department of Physics, University of Maryland, College Park, Maryland 20742, USA*
^{18}*Department of Physics and Center for Cosmology and Astro-Particle Physics, Ohio State University, Columbus, Ohio 43210, USA*
^{19}*Department of Astronomy, Ohio State University, Columbus, Ohio 43210, USA*
^{20}*Department of Physics, TU Dortmund University, D-44221 Dortmund, Germany*
^{21}*Department of Physics, University of Alberta, Edmonton, Alberta, Canada T6G 2G7*
^{22}*Department of Physics and Astronomy, University of Gent, B-9000 Gent, Belgium*
^{23}*Max-Planck-Institut für Kernphysik, D-69177 Heidelberg, Germany*
^{24}*Department of Physics and Astronomy, University of California, Irvine, California 92697, USA*
^{25}*Laboratory for High Energy Physics, École Polytechnique Fédérale, CH-1015 Lausanne, Switzerland*
^{26}*Department of Physics and Astronomy, University of Kansas, Lawrence, Kansas 66045, USA*
^{27}*Department of Astronomy, University of Wisconsin, Madison, Wisconsin 53706, USA*
^{28}*Department of Physics, University of Wisconsin, Madison, Wisconsin 53706, USA*
^{29}*Institute of Physics, University of Mainz, Staudinger Weg 7, D-55099 Mainz, Germany*
^{30}*Université de Mons, 7000 Mons, Belgium*
^{31}*Bartol Research Institute and Department of Physics and Astronomy, University of Delaware, Newark, Delaware 19716, USA*
^{32}*Department of Physics, University of Oxford, 1 Keble Road, Oxford OX1 3NP, UK*
^{33}*Department of Physics, University of Wisconsin, River Falls, Wisconsin 54022, USA*
^{34}*Oskar Klein center and Department of Physics, Stockholm University, SE-10691 Stockholm, Sweden*
^{35}*Department of Astronomy and Astrophysics, Pennsylvania State University, University Park, Pennsylvania 16802, USA*
^{36}*Department of Physics, Pennsylvania State University, University Park, Pennsylvania 16802, USA*
^{37}*Department of Physics and Astronomy, Uppsala University, Box 516, S-75120 Uppsala, Sweden*
^{38}*Department of Physics, University of Wuppertal, D-42119 Wuppertal, Germany*
^{39}*DESY, D-15735 Zeuthen, Germany*

We report on a search for extremely-high energy neutrinos with energies greater than 10^6 GeV using the data taken with the IceCube detector at the South Pole. The data was collected between April 2008 and May 2009 with the half-completed IceCube array. The absence of signal candidate events in the sample of 333.5 days of live time significantly improves model-independent limits from previous searches and allows to place a limit on the diffuse flux of cosmic neutrinos with an E^{-2} spectrum in the energy range $2.0 \times 10^6 - 6.3 \times 10^9$ GeV to a level of $E^2 \phi \leq 3.6 \times 10^{-8}$ GeV cm^{-2} sec^{-1} sr^{-1}.

I. INTRODUCTION

Cosmogenic neutrinos, the daughter particles of the Greisen-Zatsepin-Kuzmin (GZK) process in which the highest energy cosmic rays interacting with the cosmic-microwave background [1,2], may give a unique picture of the Universe in the highest energy regime. Cosmogenic neutrinos carry information about the sources of the highest energy cosmic rays, such as their location, cosmological evolution, and cosmic-ray spectra at the sources. Various cosmogenic neutrino models [3–6] which assume primary cosmic ray protons predict neutrino fluxes $E_\nu^2 \phi \geq 10^{-4}$ GeV^{-2} sec^{-1} sr^{-1} in the energy range 10^8 GeV $\leq E_\nu \leq 10^{10}$ GeV, which implies that the 4π solid angle averaged neutrino effective area divided by energy A_ν/E_ν must be larger than 10^{-5} m^2/GeV (e.g. $A_\nu \geq 10^3$ m^2 at 10^8 GeV and $A_\nu \geq 10^4$ m^2 at 10^9 GeV) to detect several cosmogenic neutrinos every year.

*Corresponding author: aya@hepburn.s.chiba-u.ac.jp (A. Ishihara)
†also Università di Bari and Sezione INFN, Dipartimento di Fisica, I-70126, Bari, Italy
‡NASA Goddard Space Flight Center, Greenbelt, MD 20771, USA

Several techniques have been used to realize such huge detection volumes for these extremely-high energy (EHE) neutrinos. Air-shower detectors search for neutrino-induced young inclined showers [7] or Earth-skimming events initiated by tau neutrinos [8]. Radio Cherenkov neutrino detectors search for radio Askar'yan pulses in a dielectric medium as the EHE neutrino signature [9–11]. Underground neutrino telescopes, such as IceCube, deployed in transparent naturally occurring media [12,13] can detect EHE neutrino interactions through the strong Cherenkov radiation emitted by the charged secondary particles. This technique is well established for observations of astrophysical neutrinos in the MeV to GeV energy region [14,15], and can also be utilized to search for cosmogenic EHE neutrinos with an appropriate background rejection method. In a neutrino telescope, an EHE neutrino interaction would be identified by the extremely-high number of Cherenkov photons deposited in the detector.

In this paper, we describe the search for neutrinos with energies above 10^6 GeV using data collected with the half-completed IceCube detector in 2008-2009. This analysis is sensitive to all three neutrino flavors. Compared to the previous EHE neutrino search described in Ref. [13], which used an earlier stage of the IceCube detector, the

current analysis benefits from the enlarged instrumented volume and from improved agreement between simulated and observed event distributions. This article presents the improved strategies implemented since the previous analysis [13].

II. DATA SETS

The analysis uses data collected from April 6, 2008 through May 20, 2009. At the time of data collection, the IceCube detector consisted of 2400 digital optical modules (DOMs) on 40 vertical strings. The volume of the detector was roughly 0.5 Km^3 with the detector center located at a depth of 1948 m below the ice surface. The DOMs consist of a 25 cm photomultiplier tube [16] with data acquisition and calibration electronics, data compression, communications, and control hardware [17]. The trigger setting was unchanged from the previous analysis [13].

The analysis was optimized on simulated data with most of the experimental data kept blind. A 10% subset of the experimental data was used for examinations of the Monte Carlo simulations and detector response. This subset comprised 35.8 days of detector live time distributed randomly throughout the data collection period, and was not used once the analysis was fully defined. The use of a statistically independent final sample conservatively ensures avoidance of possible analysis bias due to tuning a Monte Carlo simulation using an experimental subset. The selection criteria were then applied to the complementary 90% of the experimental data, comprising 333.5 days of live time.

The primary background in this analysis is muon bundles made up of large numbers of muons produced by high energy cosmic-ray interactions in the atmosphere. This background was simulated with the CORSIKA air-shower simulation package version 6.720 [18] with the SIBYLL 2.1 [19] and QGSJET-II [20] hadronic interaction models, without prompt muons from the heavy meson decays. Cosmic-ray interactions assuming pure proton and iron primary compositions in the energy region between 10^6 and 10^{10} GeV were simulated. Background contributions from primary cosmic-ray energies beyond 10^{10} GeV were estimated by extrapolation of the simulated sample up to the GZK cutoff energy of $\sim 5 \times 10^{10}$ GeV. EHE neutrino signal events in energies between 10^5 and 10^{11} GeV from several flux models [3–6,21,22] were simulated using the JULIET package [23].

III. EVENT SELECTION

The amount of energy deposited in the form of Cherenkov photons by the neutrino-induced charged particles in the detector is highly correlated with the energy of the particles [13]. An EHE neutrino interaction occurring inside or close to the IceCube detector would stand out against the background of cosmic-ray induced muons due to the much higher light deposition. The total number of photoelectrons (NPE) recorded in an event was used as the main distinctive feature to separate signal from background.

A. On-line sample

The number of photoelectrons (p.e.) recorded by an individual DOM was derived by integrating the pedestal subtracted waveforms. Each DOM has two waveform digitizers, that simultaneously capture p.e. signals with differing dynamic ranges and time windows [17]. The event total NPE was then obtained by summing the number of p.e. detected by each DOM. photomultiplier tube saturation effects and the sizes of the time windows limit the NPE estimation at high light levels. The initial NPE calculation was performed online at the South Pole. For this analysis we consider only events with $NPE_{online} \geq 630$. The event rate of this "online bright sample" was ~ 1.4 Hz. At this level, the background rate exceeded the expected signal rate by $\geq O(10^7)$.

B. Off-line sample

For the following data selection step, the NPE values were recalculated after eliminating photon signals from low energy muons accidentally coincident in a 20 μs time window of a large NPE event. These low energy muons leave a faint light, typically with an NPE < 9. The light deposition of the coinciding low energy muon was, in most cases, spatially and temporally separated from the main bright p.e. cluster. While the few coincident photons have very a small impact on the NPE calculation, they can disturb the geometrical reconstruction of the particle tracks later on in the analysis. Contributions from coincident low energy muons were eliminated by removing p.e. signals that were temporally separated from the time of the highest light deposition associated with the main high NPE event. The recording time of a p.e. signal in the i_{th} DOM, $t_{10,i}$, was defined as the time at which 10% of the total charge had been captured. The time of the highest light deposition was defined as the time t_{LN} of the DOM which captured the largest p.e. signal in the event. This time, t_{LN}, was typically associated with the time of closest approach of the charged particle tracks to any DOM in the detector. For the offline NPE calculation and track reconstruction, those p.e. signals which occurred outside the time window [− 4.4 μs, 6.4 μs] around the t_{LN} were excluded. The "offline bright sample" selects events with NPE $\geq 3.2 \times 10^3$ and the number of hit DOMs (NDOM) ≥ 200; here and below NPE and NDOM are obtained after the t_{LN} time window cleaning. These NPE and NDOM thresholds reduced the background rate by 2 orders of magnitude while keeping $\sim 70\%$ of the cosmogenic neutrino-induced events. The remaining backgrounds are bundles containing many hundreds of muons, with an estimated cosmic-ray energy above 10^7 GeV.

C. Quality cut

Apart from NPE, the particle direction and the depth distribution of the detected Cherenkov photons are distinctive event features that separate the EHE neutrino signal from the atmospheric muon background. Because of the energy dependence of the neutrino interaction cross section, most of the EHE neutrino signal is expected from directions close to the horizon. As a result of the depth dependence of the optical properties of the Polar ice, the largest photon signals are often detected in the deepest part of the detector, where the ice is most transparent [24]. On the other hand, the background atmospheric muons enter the detection volume from above and lose a substantial fraction of their energy during propagation through the detector. Therefore, the time and depth coordinates, z, of the detected Cherenkov photons, measured relative to the detector center, show negative correlation for background. The largest photon signals from these background muons are expected at shallow depths near the top of the detector. Exceptions are inclined atmospheric muon bundles that pass outside the instrumented volume with the point of closest approach in the deep, clear ice at the bottom of the detector, or individual muons that deposit most of their energy in an isolated catastrophic energy loss in the deep ice after having passed through the top part of the detector. Track reconstructions often fail to identify such atmospheric muon events as downward-going tracks, when most of the light deposition occurs in the deep part of the detector. Therefore, a track reconstruction is applied only to those events in which the DOM with the largest signal is located at $z > -300$ m ("shallow events"). The negative z value indicates the vertical distance below the center of the IceCube detector. For events with the largest photon signal at $z < -300$ m ("deep events"), further event selection criteria rely on timing instead of directional information.

For the shallow events, the particle directions are reconstructed with the LineFit algorithm [13]. Since the majority

of the EHE neutrino-induced events is close to the horizon [23] while the directions of the background muon bundles are mostly vertical, it is important to minimize the number of background tracks that are misreconstructed as horizontal. In order to reject the misreconstructed background events, another simple one-dimensional reconstruction is introduced. The distribution of average depth of p.e. as a function of timing is fitted by a linear function, $\bar{z}(t_{10}) = C_0 + S_{zt} \cdot t_{10}$. The fit parameter, S_{zt}, is a measure for the speed at which the light signal propagates in z-direction, and hence for the inclination of the tracks. For vertically downward-going relativistic particles, the quantity S_{zt}/c takes values ~ -1, where c is the vacuum speed of light, whereas close to horizontal tracks yield values $S_{zt}/c \sim 0$. The shallow "quality bright sample" requires an additional condition of $(S_{zt}/c + \cos\theta) \geq -0.4$ where θ is the reconstructed zenith angle from the LineFit. This condition excludes events for which the one-dimensional fit suggests a significantly more vertical downward-going geometry than the LineFit. Both signal and background are reduced by less than $\sim 2\%$ by this criterion. Figure 1 shows the distributions of NPE (panel (a)) and $\cos\theta$ (panel (b)) for experimental data, background and signal simulations in the quality bright sample. The distributions of CORSIKA-SIBYLL with an iron primary composition show a reasonable agreement with experimental data while the total event rates are 50% overestimated by simulation. The zenith angle reconstruction resolution of the shallow quality bright sample is $\sim 1.4°$ root mean square for muon bundle background and $\geq \sim 2.5°$ for ν_μ signal. This is because the ν_μ signal experiences more stochastic energy losses along with hadronic cascades at its interaction vertices.

The deep bright events ($Z_{LN} \leq -300$ m) are mostly events that traverse the bottom edge of IceCube or are uncontained events that propagate or cascade below the detector. The inclination of these events tends to be reconstructed more horizontally than the true direction. The
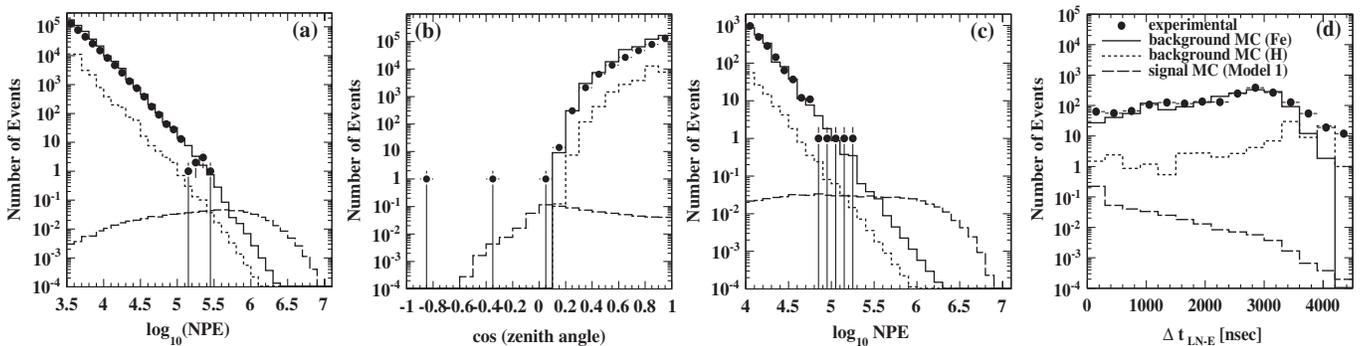

FIG. 1.   Event observables in the quality bright sample that are used for the final selection criteria. Distributions of (a) NPE and (b) cosine of the reconstructed zenith angle for shallow events, and (c) NPE and (d) Δt_{LN-E} for deep events in a live time of 333.5 days. The black circles represent experimental data and the solid and dashed lines are CORSIKA-SIBYLL with iron and proton primaries, respectively. The expected signal distributions from simulations of the GZK 1 model (sum of all three neutrino flavors) are shown as long-dashed histograms. Systematic uncertainties are not included.
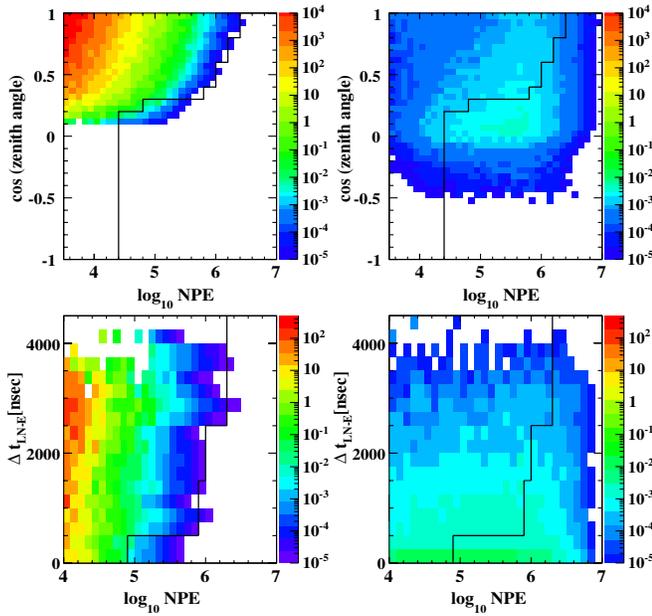
FIG. 2 (color online).   Event number distributions of the shallow (upper panels) and deep (lower panels) quality bright sample in 333.5 days are shown for the background (left panels) and signal (right panels) simulations. The signal distributions are from GZK 1 model [3] adding all three flavors of neutrinos. The background distributions are from CORSIKA-SIBYLL with iron primaries. The series of thick lines in each panel indicate the final sample selection criteria.

agreement between the simulation and experimental distributions improves with increasing NPE threshold values for these events. Events with NPE $\leq 10^4$ are discarded from the deep quality bright sample in order to achieve a reasonable agreement between experimental data and simulations. Since the majority of the EHE neutrino-induced events have NPE $\geq 10^4$, the effect on the signal efficiency by this requirement is minimal. A fraction of 96% of background is rejected by the cut, while 91% of the signal is retained. Panel (c) in Fig. 1 shows the NPE distributions from the deep quality bright sample.

D. Final selection

The final event selection is chosen in order to minimize the model discovery factor (MDF = $\mu_{\mathrm{lds}}/N_{\mathrm{signal}}$) [25] in

the region of the phase space where a better signal to background ratio (S/B) is expected, where μ_{lds} is the least number of events to claim signal discovery at 5σ significance and N_{signal} is the number of neutrinos expected from the GZK 1 [3] model flux. For the shallow events, high S/B is obtained in the region near the horizontal reconstructed direction as shown in Fig. 1(b). For the deep events, instead of reconstructing the inclination of events, we utilize the time interval, $\Delta t_{\mathrm{LN-E}}$, between the earliest detected photon in an event and t_{LN} to obtain the best S/B subsample. The vertical atmospheric muon bundle events with the largest number of p.e. near the bottom of IceCube are often associated with a small number of p.e. in the shallow detector region much earlier than t_{LN}. This contrasts to the EHE neutrino signal events. The main contributions to a detectable EHE signal in IceCube come from neutrino-induced horizontal muons and taus [23]. These produce the largest number of p.e. signals shortly after the first recorded photoelectrons. Contained cascadelike events induced by neutrino interactions [26] inside the IceCube detector volume also exhibit a similar trend. Figure 1(d) shows the distributions in the deep quality bright sample. The best S/B is achieved in the bin $\Delta t_{\mathrm{LN-E}} \sim 0$ ns. The high rate in the experimental data for $\Delta t_{\mathrm{LN-E}} \geq 3600$ is due to random noise in the DOMs and remaining coincident muons that were underestimated by the simulations. The slightly higher rate for the data in the bin $\Delta t_{\mathrm{LN-E}} \sim 0$ ns may reflect the fact that the ice is cleaner than what was simulated in the deep region. Figure 2 presents the event distributions in the planes of $\cos\theta$ vs NPE for the shallow events and $\Delta t_{\mathrm{LN-E}}$ vs NPE for the deep events. Optimization is performed by differentiating the NPE threshold numbers in the region $\cos\theta \leq 0.3$ or $\Delta t_{\mathrm{LN-E}} \leq 0.5~\mu$s for the shallow and deep quality bright sample, respectively. The NPE threshold of the other region ($\cos\theta \geq 0.3$ or $\Delta t_{\mathrm{LN-E}} \geq 0.5~\mu$s) is conservatively determined such that the number of background events above the threshold is less than 10^{-4} of the full live time for each bin of $\cos\theta$ with width 0.2 or 1 μs for $\Delta t_{\mathrm{LN-E}}$. This improves the detection sensitivity without sacrificing discovery potential. The solid lines in Fig. 2 are the final level selection criteria determined from the background (CORSIKA-SIBYLL, iron) and signal (GZK 1 [3]) Monte Carlo simulations following a blind analysis strategy. The minimum NPE

TABLE I.   Number of events passing cuts at various selection levels with 333.5 days detector live time. The signal rates correspond to simulations of the GZK 1 model [3]. The errors of the online, offline and quality bright samples are statistical only. Systematic uncertainties in the expected event rates at the final selection level are given as asymmetric error intervals after the statistical error.

Samples	Experimental		Background MC (SIBYLL, iron)		Signal MC (GZK 1)	
On-line	3.7×10^7		$(3.8 \pm 0.1) \times 10^7$		1.8 ± 0.007	
Off-line	3.3×10^5		$(4.8 \pm 0.2) \times 10^5$		1.2 ± 0.006	
	Shallow	Deep	Shallow	Deep	Shallow	Deep
Quality	2.9×10^5	1.9×10^3	$(4.4 \pm 0.2) \times 10^5$	$(1.7 \pm 0.2) \times 10^3$	0.76 ± 0.005	0.43 ± 0.004
Final	0	0	$0.076 \pm 0.012^{+0.051}_{-0.075}$	$0.032 \pm 0.010^{+0.022}_{-0.032}$	$0.39 \pm 0.004^{+0.054}_{-0.043}$	$0.18 \pm 0.002^{+0.025}_{-0.020}$

threshold value is 2.5×10^4. Events with NPE above the threshold value in each bin are considered to be signal event candidates. No events above the threshold are found in the 10% subset of the experimental sample. Monte Carlo simulations indicate that a cosmic-ray primary energy of at least $\sim 2 \times 10^9$ GeV is required for a muon bundle to be selected as the final sample. Table I summarizes the number of events retained in each level of analysis.

IV. THE SYSTEMATICS

Table II summarizes the sources of statistical and systematic errors in signal and background. The systematic uncertainties are assumed to have a flat distribution and are summed in quadrature separately for background and signal.

The dominant source of systematic uncertainty in the signal event rate is the relationship between the measured NPE and the energy of the charged particles. The uncertainty is estimated by calibrating the absolute sensitivity of the DOMs in the laboratory and by calibrating the *in-situ* sensitivity using light sources codeployed with the DOMs in the ice. The estimation by the latter method involves systematic errors in the simulation of the photon propagation in the ice. The uncertainty associated with possible underestimation in the DOM's random noise is estimated by adding artificial random photoelectrons into 10% of the simulated events. The other uncertainties attributed to the neutrino interactions [27] and their daughters' interactions in the ice are similarly estimated as in the previous analysis [13].

TABLE II. List of the statistical and systematic errors for signal (top) and background (bottom) simulations. The uncertainties for the signal are listed relative to the rate estimated for GZK 1 [3]. The uncertainties in the signal rates vary with assumed signal spectra. The uncertainties in the background rate are estimated with CORSIKA-SIBYLL assuming iron composition.

Sources	Signal rate (%)
Statistical error	± 0.8
NPE	$+3.9 / -7.2$
Noise	-1.8
Neutrino cross section	± 9.0
Photo-nuclear interaction	$+10.0$
Landau-Pomeranchuk-Migdal effect	± 1.0
Total:	$\pm 0.8(\text{stat}) + 14.0 - 11.7(\text{sys})$

Sources	Background rate (%)
Statistical error	± 17.0
NPE	$+37.1 / -46.7$
Noise	-2.2
Cosmic ray composition	-83.9
Hadronic interaction model	$+36.1$
Coincident events	$+31.2$
Total:	$\pm 17.0(\text{stat}) + 60.4 - 96.0(\text{sys})$

The dominant source of systematic uncertainty in the background event rates arises from the uncertainty in the primary cosmic-ray composition at the relevant energies ($> 10^7$ GeV) and the hadronic interaction model used in the simulation of the air showers. The systematic uncertainty associated with the cosmic-ray composition is evaluated by considering two extreme cases of atmospheric muon simulations with either pure iron or pure proton primary compositions. Similarly, the uncertainty due to the hadronic interaction model is evaluated using atmospheric muon simulations with two different high energy hadronic interaction models: SIBYLL 2.1 and QGSJET-II. Systematic uncertainties associated with the NPE measurement and the possible DOM noise rate underestimation are determined in the same manner as for signal events. The background contribution from possible prompt muons created in decays of charmed mesons is negligible. There is also uncertainty due to statistical limitations of the simulated coincident muon sample at NPE $\geq 10^4$. This error is estimated by extrapolating distributions of statistically richer lower NPE coincident simulation events to the final selection region. Possible coincident events in the final sample are also estimated by the temporally and geometrically separated p.e. signals from the main p.e. cluster in each event. This coincident event check suggested that one of the two upward-going reconstructed events in Fig. 1(b) at $\cos\theta = -0.38$ was due to coincident muons. The other upward-going event ($\cos\theta = -0.83$) was possibly neutrino-induced, while the NPE values of both events were approximately 4300 p.e., a factor of 6 less than the final threshold value.

V. RESULTS

No events in the blinded 90% experimental data pass all the selection criteria. This is consistent with the expected background level of $0.11 \pm 0.02^{+0.06}_{-0.10}$ events in a live time of 333.5 days. The passing rates for experimental and simulated events at each selection level are listed in Table I.

The quasidifferential model-independent 90% CL limit on neutrino fluxes [28] normalized by energy decade is shown in Fig. 3 assuming full mixing in the standard neutrino flavor oscillation scenario. In the limit calculation, the energy decade averaged effective area is used and the contribution from the Glashow resonance [29] is neglected. Incorporating the statistical and systematic uncertainties, the background is expected to be found with a uniform prior probability between 0 and 0.19. These uncertainties are included in the final limit using a method outlined in [30]. This estimation together with the null result in the experimental sample gives the Feldman-Cousins 90% CL event upper limit [31] of 2.35 events. For cosmic neutrinos with an E^{-2} energy spectrum, this implies an integral flux limit of $E^2 \phi \leq 3.6 \times 10^{-8}$ GeV cm^{-2} sec^{-1} sr^{-1} with the central 90% of the E^{-2} signal found in the energy interval
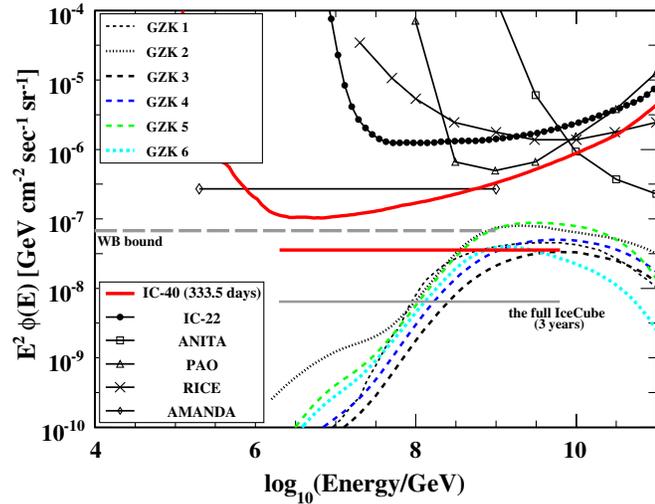
FIG. 3 (color online). All flavor neutrino flux differential limit and E^{-2} spectrum integrated limit from the 2008-2009 IceCube EHE analysis (bold solid lines). The systematic errors are included. Various model predictions (assuming primary protons) are shown for comparison: GZK 1 $((m, Z_{max}) = (4, 4))$ [3], GZK 2 [4], GZK 3 $(\Omega_\Lambda = 0.0)$, GZK 4 $(\Omega_\Lambda = 0.7)$ [5], GZK 5 (maximal) and GZK 6 (the best fit, incorporating the Fermi-LAT bound) [6]. The gray dashed horizontal line indicates the Waxman-Bahcall flux bound with cosmological evolution [32]. Model fluxes are summed over all neutrino flavors, assuming standard neutrino oscillations. The model-independent differential upper limits by other experiments are also shown for Auger (PAO) [8], RICE [9], ANITA [11], and the previous IceCube result (IC22) [13]. Limits from other experiments are converted to the all flavor limit assuming standard neutrino oscillation and a 90% quasidifferential limit when necessary. The integral flux limit on a pure E^{-2} spectrum is shown for AMANDA-II [12]. For reference, the estimated integrated limit for three years of observation with the full IceCube detector with the same analysis strategy is denoted as a gray solid line.

$2.0 \times 10^6 - 6.3 \times 10^9$ GeV. This result is the first constraint of neutrino fluxes below the Waxman-Bahcall (WB) flux bound [32] in this energy region.

VI. DISCUSSIONS AND SUMMARY

We analyzed the 2008-09 data sample collected by the 40-string IceCube detector to search for extremely-high energy neutrinos with energies exceeding 10^6 GeV. The differential and integral limits obtained are significantly improved relative to our previous result [13]. This is due to both the increased instrumented volume and improvements of the Monte Carlo simulations. The improved agreement between experimental and simulated data allowed a loosening of the NPE threshold in the data selection, thereby lowering the energy threshold of the analysis and improving the selection efficiency for high energy signal events that occurred outside the instrumented volume. This can also be seen in the corresponding neutrino effective area at the final selection shown in Fig. 4. Compared to the
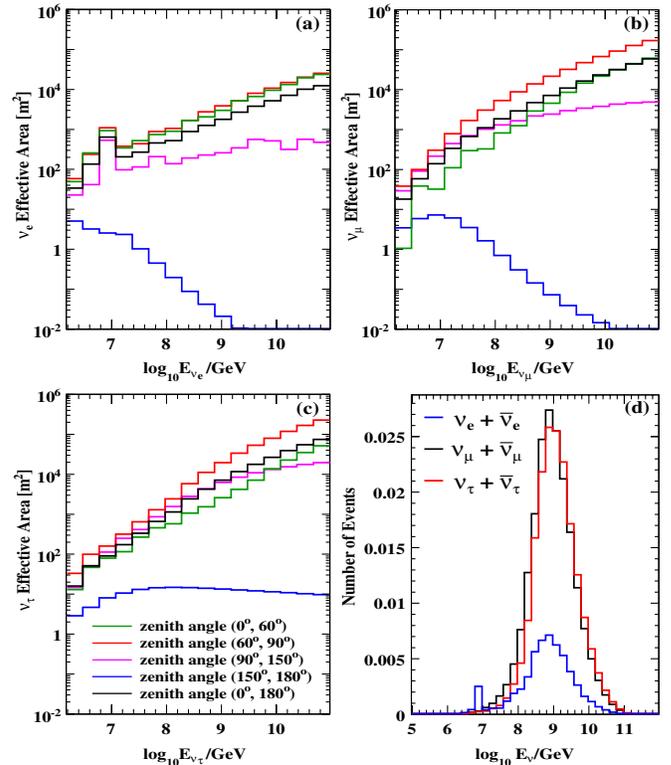

FIG. 4 (color online). Solid angle averaged neutrino effective area for four declination bands as well as that of the full solid angle average for (a) $\nu_e + \bar{\nu}_e$ (b) $\nu_\mu + \bar{\nu}_\mu$ and (c) $\nu_\tau + \bar{\nu}_\tau$, assuming equal flux of neutrinos and antineutrinos. The lower right plot shows the final level signal event distributions for 333.5 days with the GZK 6 model spectra [6] for each neutrino flavor.

previous search [13], the effective area is a factor of 6 and 3.3 increased at 3×10^7 GeV and 10^9 GeV, respectively. The full solid angle averaged 3 flavor (assuming $\nu_e : \nu_\mu : \nu_\tau : = 1:1:1$) neutrino effective area reaches 300 m² at 10^8 GeV and 2100 m² at 10^9 GeV. The 90% CL differential limit at 10^9 GeV is a factor of ~4 higher than the fluxes predicted by the models GZK 2 and 5, and a factor of ~8 higher than the flux predicted by the models GZK 1, 4, 6, all of which assume primary protons. This suggests that the IceCube EHE neutrino search will reach these flux levels in the near future since the event rate is roughly proportional to the fiducial volume (see Fig. 3), and the current analysis used only the half-instrumented IceCube detector configuration. Further improvements in sensitivity would enable IceCube to act as a probe of the primary cosmic ray composition at GZK energies [33].

Figure 4 indicates that a large part of the EHE neutrino signal is expected from the zenith angle region between 60° and 90°. Upward-going EHE neutrinos are absorbed in the Earth. The propagation length of secondary muons and taus is greater than the distance between the surface and the IceCube fiducial volume. Thus, the inclined particles that reach the IceCube detector are created in the Earth. For ν_e,

TABLE III. Expected number of events in 333.5 days from several cosmogenic neutrino models and top-down models. The confidence interval for exclusion by this observations is also listed where appropriate. The cosmogenic neutrino models (GZK 1-6) assume the cosmic-ray primaries to be protons and different spectral indices/cutoff energies at sources as well as different cosmological evolution parameters and extension in redshift for the sources. Representative models with moderate (GZK 3, 4, 6), moderately strong (GZK 1) and strong (GZK 2, 5) source evolution parameters are listed here.

Models	Event rate	C.L. %
GZK 1 [3]	0.57	$\cdots$
GZK 2 [4]	0.91	53.4
GZK 3 ($\Omega_\Lambda = 0.0$) [5]	0.29	$\cdots$
GZK 4 ($\Omega_\Lambda = 0.7$) [5]	0.47	$\cdots$
GZK 5 (maximal) [6]	0.89	52.8
GZK 6 (the best fit) [6]	0.43	$\cdots$
Top-down 1 (SUSY) [22]	1.0	55.7
Top-down 2 (no-SUSY) [22]	5.7	99.6
Z-burst [21]	1.2	66.4
WB bound (with evolution) [32]	4.5	$\cdots$
WB bound (without evolution) [32]	1.0	$\cdots$

the event signatures are produced nearly at the neutrino interaction points and the current analysis is sensitive to all downward-going geometries. The peaked features in Fig. 4 (a) and 4(d) at $E_{\nu_e} \sim 6.3$ PeV are due to the Glashow resonance [29]. Expected signal energy distributions of GZK 6 at the final selection level are shown in the lower right panel in Fig. 4. The peak energy of the expected signal after all selection criteria is at $\sim 7.0 \times 10^8$ GeV. Significant contributions from all neutrino flavors are observed. In the GZK 6 model, 13% of the signal are from ν_e, 45% are from ν_μ and 42% are from ν_τ. Through-going tracks (muons and taus) constitute 60% of the signal rate and the rest are neutrino interactions that create cascadelike events near and inside the detector volume. Table III gives the event rates for several model fluxes of

cosmogenic neutrinos, top-down scenarios, and a pure E^{-2} power-law neutrino spectrum normalized to the Waxman-Bahcall flux bounds for reference. We expect 0.3 to 0.9 cosmogenic neutrino events in 333.5 days, assuming moderate to strong cosmological source evolution models. The half-instrumented IceCube detector is already capable of constraining those models with relatively high neutrino fluxes. The IceCube sensitivity to cosmological EHE neutrinos continues to grow.

[1] K. Greisen, Phys. Rev. Lett. **16**, 748 (1966); G. T. Zatsepin and V. A. Kuzmin, Pis'ma Zh. Eksp. Teor. Fiz. **4**, 114 (1966); [JETP Lett. **4**, 78 (1966)].

[2] V. S. Berezinsky and G. T. Zatsepin, Phys. Lett. B **28**, 423 (1969).

[3] S. Yoshida and M. Teshima, Prog. Theor. Phys. **89**, 833 (1993); The model with the source evolution $(z_{\max} + 1)^m$ with $m = 4$ extending to $z_{\max} = 4.0$.

[4] O. E. Kalashev, V. A. Kuzmin, D. V. Semikoz, and G. Sigl, Phys. Rev. D **66**, 063004 (2002).

[5] R. Engel, D. Seckel, and T. Stanev, Phys. Rev. D **64**, 093010 (2001).

[6] M. Ahlers *et al.*, Astropart. Phys. **34**, 106 (2010).

[7] R. U. Abassi *et al.* (HiRes Collaboration), Astrophys. J. **684**, 790 (2008).

[8] J. Abraham *et al.* (Pierre Auger Collaboration), Phys. Rev. D **79**, 102001 (2009); (Private communications).

[9] I. Kravchenko *et al.* (Rice Collaboration), Phys. Rev. D **73**, 082002 (2006).

[10] P. W. Gorham *et al.* (GLUE Collaboration), Phys. Rev. Lett. **93**, 041101 (2004).

[11] P. W. Gorham *et al.* (ANITA Collaboration), Phys. Rev. D **82**, 022004 (2010); arXiv:1011.5004 (erratum).

[12] M. Ackermann *et al.* (IceCube Collaboration), Astrophys. J. **675**, 1014 (2008).

[13] R. Abbasi *et al.* (IceCube Collaboration), Phys. Rev. D **82**, 072003 (2010).

[14] K. Hirata *et al.*, Phys. Rev. Lett. **58**, 1490 (1987); Y. Fukuda *et al.* (Kamiokande Collaboration), Phys. Rev. Lett. **77**, 1683 (1996); Y. Fukuda *et al.* (Super-Kamiokande Collaboration), Phys. Rev. Lett. **81**, 1158 (1998).

[15] Q. R. Ahmad *et al.* (SNO collaboration), Phys. Rev. Lett. **87**, 071301 (2001).

[16] R. Abbasi *et al.* (IceCube Collaboration), Nucl. Instrum. Methods Phys. Res., Sect. A **618**, 139 (2010).

[17] R. Abbasi *et al.* (IceCube Collaboration), Nucl. Instrum. Methods Phys. Res., Sect. A **601**, 294 (2009).

[18] D. Heck *et al.*, Forschungszentrum Karlsruhe Report FZKA 6019, 1998.

[19] E. J. Ahn, R. Engel, T. K. Gaisser, P. Lipari, and T. Stanev, Phys. Rev. D **80**, 094003 (2009).

[20] S. Ostapchenko, Phys. Rev. D **74**, 014026 (2006); Nucl. Phys. B, Proc. Suppl. **151**, 143 (2006).

[21] S. Yoshida, G. Sigl, and S. Lee, Phys. Rev. Lett. **81**, 5505 (1998).

[22] G. Sigl *et al.*, Phys. Rev. D **59**, 043504 (1998).

[23] S. Yoshida *et al.*, Phys. Rev. D **69**, 103004 (2004).

[24] M. Ackermann *et al.*, J. Geophys. Res. **111**, D13203 (2006).

[25] G. C. Hill *et al.*, in *the Proceedings of PHYSTAT2005, Oxford, England, 2005* (Imperial College Press, London, 2006), pp 108–111.

[26] R. Abbasi *et al.* (IceCube Collaboration), arXiv:1101.1692 [Phys. Rev. D. (to be published)].

[27] A. Cooper-Sarkar and S. Sarkar, J. High Energy Phys. 01 (2008) 075.

[28] L. A. Anchordoqui *et al.*, Phys. Rev. D **66**, 103002 (2002).

[29] S. L. Glashow, Phys. Rev. **118**, 316 (1960).

[30] F. Tegenfeldt and J. Conrad, Nucl. Instrum. Methods Phys. Res., Sect. A **539**, 407 (2005).

[31] G. J. Feldman and R. D. Cousins, Phys. Rev. D **57**, 3873 (1998).

[32] E. Waxman and J. Bahcall, Phys. Rev. D **59**, 023002 (1998); S. Razzaque, P. Meszaros, and E. Waxman, Phys. Rev. D **68**, 083001 (2003).

[33] L. A. Anchordoqui, H. Goldberg, D. Hooper, S. Sarkar, and A. M. Taylor, Phys. Rev. D **76**, 123008 (2007).